



Composite Based on Babassu (*Orbignya* Sp.) Mesocarp Residue and Palygorskite as Bioplastic

Moisés das Virgens Santana^{1,7} · Railson Machado Pinto¹ · Emanuel Airton de Oliveira Farias¹ · Kariny da Rocha Alves¹ · Cristiany Marinho Araújo² · Cristiano José de Farias Braz³ · Renata Barbosa⁶ · Tatianny Soares Alves⁶ · Luiz Carlos Bertolino^{4,5} · Carla Eiras¹

Accepted: 21 September 2023

© The Author(s), under exclusive licence to Springer Science+Business Media, LLC, part of Springer Nature 2023

Abstract

The solid waste generated by the disposal of plastic materials has become one of society's major problems in recent years. In this sense, several researchers have sought alternatives to minimize environmental pollution. A promising option would be using natural materials, biopolymers, or a mixture of these, also known as composites. In this study, composite films were prepared based on babassu mesocarp (BM) and palygorskite clay mineral (Pal), using the casting technique, as well as the plasticizers sodium alginate (SA) and glycerol (Gl). The films obtained were called BM/SA/Gl/Pal, and for comparison were, prepared films containing BM and BM/SA/Gl. The films presented uniform color, smooth and shiny surfaces, and no fissures. FTIR analysis indicated possible interactions between clay and matrix. The SEM analysis showed that the BM film presented more significant surface irregularity. In contrast, the BM/SA/Gl/Pal film gave a more regular topography and excellent thermal stability. Finally, the BM/SA/Gl/Pal film showed more promising results when compared to the others and is considered an attractive material for use in biodegradable packaging.

Keywords Biocomposite · Attapulgitite, and autossuported films

✉ Carla Eiras
eirasc@ufpi.edu.br

- ¹ Laboratório de Pesquisa e Desenvolvimento de Novos Materiais e Sistemas Sensores (MATSENS), Universidade Federal do Piauí, Teresina 64049-550, Piauí, Brazil
- ² Federal de Educação, Ciência e Tecnologia do Piauí (IFPI), Campus Zona Sul, Teresina 64018-900, Piauí, Brazil
- ³ Programa de Pós-Graduação em Ciência e Engenharia de Materiais, Universidade Federal de Campina Grande (UFCG), Paraíba, Brasil
- ⁴ Faculdade de Geologia, Universidade do Estado do Rio de Janeiro – UERJ, Rua São Francisco Xavier, 524 – Maracanã, Rio de Janeiro 550-900, Brazil
- ⁵ Faculdade de Geologia (FGEL), Universidade do Estado do Rio de Janeiro, 20.550-900, Rio de Janeiro, Brazil
- ⁶ Laboratório de Polímeros e Materiais Conjugados (LAPCON), Universidade Federal do Piauí, Teresina 64049-550, Piauí, Brazil
- ⁷ Programa de Pós-Graduação em Ciências e Engenharia dos Materiais, Universidade Federal do Piauí (UFPI), Teresina 64049-550, Piauí, Brasil

Introduction

The use of plastics combined with new technologies and the increase in consumption by the population has become one of the major problems of the contemporary world. This fact is due to the rise in solid waste production since most of these remain in for hundreds of years in the environment until they are degraded [1, 2].

Thermoplastics have many applications; they are very present in everyday life, from disposable and cheap products, such as bags or films for packaging, bottles, appliances, and automotive accessories [3]. In Brazil, the amount of municipal solid waste generated is estimated to be around 229.2 thousand tons per day, but only 1.3% of this total is recycled [4].

Due to the problems caused by synthetic polymers [5], many alternatives have been proposed to minimize the environmental impacts caused by plastic products' rampant use and improper disposal. Such studies are based on producing and using biopolymers or natural polymers, which emerge as an alternative in technological applications to collaborate with the planet's sustainable development [6].

Natural composites based on biopolymers such as proteins and polysaccharides are considered possible substitutes for non-biodegradable petroleum-based polymers, for example, in food packaging and plastic bags [7]. There is, therefore, a need to develop sustainable, biodegradable materials [8].

Among the various biodegradable materials of natural origin, polysaccharides or biopolymers stand out due to their natural abundance, obtained from plant or animal sources. In addition, they have a low cost of acquiring and allow chemical changes in their structure [9, 10]. Different biopolymers like starch have been used to develop films [11]. Due to its ability to form films, starch has been widely studied in packaging development. It can be obtained from different sources such as corn, wheat, potato, rice, and babassu coconut mesocarp flour [12].

Babassu trees (*Orbignya* sp) (Fig. 1A) are abundant in the Brazilian region known as Mata dos Cocais, occupying about 196 thousand km² of Brazilian territory, occurring in the states of Maranhão, Tocantins, and Piauí. The babassu fruit (Fig. 1B) comprises the epicarp (11%), mesocarp (23%), endocarp (59%), and almond (7%) [13]. It is possible to extract oil from the babassu almond, the main product obtained from babassu, used in the oleochemical, cosmetic, biofuel, and food industries. Other parts of the babassu fruit (epicarp, mesocarp, and endocarp) have great potential for producing charcoal, tar, fuel gas, starch, and alcohol. On the other hand, babassu mesocarp is a by-product of babassu oil extraction; it is generated during the separation of the babassu seed. The drying and grinding of the mesocarp give rise to flour (Fig. 1C), which has a high concentration of starch, about 68%, making it feasible to use in producing films for packaging. Therefore, it would be interesting to use this starch source, mainly due to its low cost of obtaining and the possibility of adding value to this regional material that is usually discarded after the extraction of babassu coconut kernels [14].

One of the Babassu Mesocarp (BM) applications attracting interest is its use in producing biodegradable films using the casting technique [14]. Film preparation using the casting technique requires adding other materials to improve

the mechanical properties of the films, such as their tensile strength. In this sense, an alternative to enhance the mechanical properties of babassu mesocarp films may be the insertion of plasticizers such as glycerol, sorbitol, or alginate to improve plasticity and a clay mineral, acting as a charge in the polymeric matrix [15, 16]. Besides, clay minerals are materials used to reinforce plastics or rubber properties [17].

The clay mineral palygorskite (Pal) (Fig. 1D) is a hydrated aluminum and magnesium silicate with reactive hydroxy groups on the surface ($\text{Si}_8\text{Mg}_5\text{O}_{20}(\text{OH})_2(\text{OH})_4 \cdot 4\text{H}_2\text{O}$). Pal is a non-planar clay mineral with an open channel structure, forming elongated crystals and fibrous morphology of the 2:1. It has a double layer of silicon tetrahedron and a central layer of magnesium, aluminum, or iron octahedron. Furthermore, this clay mineral is widely available in Piauí [18, 19].

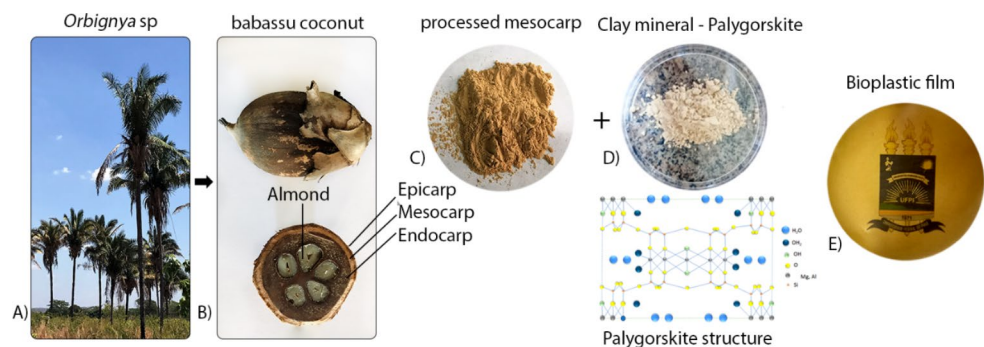
Therefore, this study aims to develop and characterize films by casting from a composite based on babassu mesocarp associated with palygorskite clay and plasticizers, glycerol, and sodium alginate for future applications such as biodegradable packaging.

Materials and Methods

Materials

The babassu coconut mesocarp produced films via casting, serving as the films' polymeric matrix. As plasticizing agents, sodium alginate (90%, Synth) and glycerol (99%, Impex) were obtained commercially and with an analytical degree. The babassu coconut mesocarp, in powder form, was supplied by the Center for Agricultural Sciences of the Universidade Federal do Piauí (UFPI), located at Teresina City, in Piauí State. Palygorskite, the clay mineral used in this study, came from the municipality of Guadalupe - PI and was obtained commercially.

Fig. 1 Primary materials used in the production of bioplastic film



Processing of Palygorskite

Pal samples were macerated and passed through a 200 mesh (0.074 mm) sieve, vendor Pavitest (NBR NM ISO 3310/1). Subsequently, successive washings were performed with ultrapure water from the Milli-Q system. After each wash, samples were centrifuged (Nova Instruments, model NI 1812) for three minutes at a speed of 5000 rpm. Finally, they were dried in an oven vendor Tecnal (TE-393/80L) at 60 °C, then macerated and sieved.

Films Composition

The optimized conditions for obtaining the film based on babassu mesocarp (BM), Palygorskite (Pal), sodium alginate (SA), and glycerol (GI) are summarized in Table 1. Other configurations tested in the search for obtaining the films of interest are shown in the supplementary material (Table S1). Thus, the best film, BM/SA/GI/Pal, was obtained with 10% glycerol and a 3:1 (m/m) ratio between BM and SA. According to other studies, the Pal concentration was fixed at 5% since higher concentrations can make the film brittle [20, 21].

Preparation of Films by Casting

The components were added to 30 mL of distilled water and subjected to mechanical agitation (Vendor velp arex-F20500413) for 30 min at 900 rpm, as illustrated in Fig. S1 (supplementary material). After 30 min of stirring at room temperature (24 °C), the solution was heated to 80 °C for 30 min in a mechanical agitator. Subsequently, the solutions were transferred to a Petri dish and taken at 40 °C for 24 h for solvent evaporation. Films were produced in triplicate and stored at room temperature for subsequent characterization.

Fourier Transform Infrared Spectroscopy (FTIR)

Fourier transform infrared spectra, using ATR, were obtained using a Spectrum 100 spectrometer (Perkin Elmer), after 16 scans, in the 4000–650 cm⁻¹.

Table 1 Optimized proportions of babassu mesocarp, sodium alginate, glycerol, and Palygorskite for film obtention

Films	BM (g)	SA (g)	GI (g)	Pal (g)	H ₂ O (mL)
BM	0.800	0.000	0.000	0.000	20
BM/SA/GI	0.300	0.100	0.040	0.000	30
BM/SA/GI/Pal	0.300	0.100	0.040	0.020	30

Scanning Electron Microscopy (SEM)

The scanning electron microscope used in the morphological analysis was in a scanning electron microscope (SEM) with a field emission gun, brand FEI, model Quanta FEG250, with acceleration voltage from 1 to 30 kV, equipped with a chemical microanalysis system by energy dispersion (EDS), Bruker (Quantax). The samples were coated with silver before each analysis.

Thermal Analysis

The Thermogravimetric Analysis (TGA), and the Derived Thermogravimetric Analysis (DTGA) were carried out using Netzsch STA (model 449 C). The samples were heated using a heating rate of 20 °C/min and a temperature range of 20 to 800 °C under a nitrogen atmosphere and a 20 mL/min flow.

Mechanical Test

The ASTM (model D882-12) was used to obtain tensile strength and elongation at break measurements. The tests were conducted at room temperature, 50 mm/min speed, and quintuplicate. The mechanical tests were carried out in an Emic mechanical testing machine (model DL 1000), with a load cell of 20 kgf. The samples had dimensions of 10 cm in length and, 1 cm in width and 0.07 mm in average thickness. Ten measurements were obtained for each sample with a crosshead speed of 50 mm/min and claw spacing of 2.5 cm.

Moisture Content

The moisture content (MC) measurement was performed for the films with glycerol in samples with dimensions of 20 mm x 20 mm; initially, the initial mass of each film (M_i) was determined, then the films were dried in an oven for 24 h at 105 °C. Subsequently, the final mass of the films (M_f) was determined; therefore, the measurements were carried out in triplicate, and the average values were used in Eq. (1) to determine the moisture content.

$$M_C (\%) = (M_i - M_f) / M_i * 100 \quad (\text{Eq. 1})$$

Water Solubility

Initially, the initial mass (M_o) of the films was determined in the dimensions of 20 mm x 20 mm; then, the films were immersed in 30 mL of distilled water and stirred on a stirring table, (Orbital SL – 180/D), for a period of 24 h at 180 rpm.

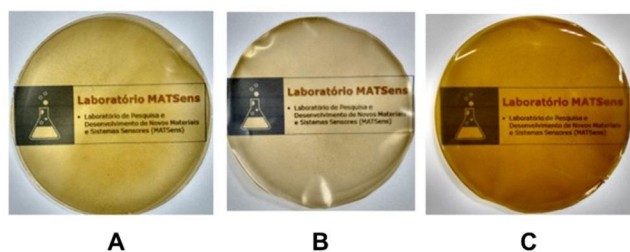


Fig. 2 The visual aspect of the films: (A) BM; (B) BM/SA/Gl; (C) BM/SA/Gl/Pal

After this period, the samples were dried in an oven at 105 °C for 24 h. Finally, the final mass (M_f) of each sample was determined, as well as film water solubility (S_W) using Eq. (2) (in triplicate).

$$S_W (\%) = (M_o - M_f) / M_o * 100 \quad (\text{Eq. 2})$$

Wettability

The wettability of the films was analyzed using a contact angle meter from Software CAM 2008 KSV Instruments. A volume of 16.0 μL was used for the analysis, referring to a small drop of distilled water deposited on each sample's surface. Later, images of the drop's interaction with the sample's surface were captured and analyzed by the Cam2008 software. Finally, each film's average contact angle and standard deviation were determined.

Results and Discussion

Visual Appearance Analysis

The images of the films produced from BM, BM/SA/Gl, and BM/SA/Gl/Pal are shown in Fig. 2 (A, B, and C), respectively.

According to the images in Fig. 2, the films presented a homogeneous visual without insoluble particles, bubbles, and uniform color. The films presented a continuous appearance without brittle areas or breaks. In addition to being transparent, they exhibited a smooth surface, facilitating their handling and removal from the Petri dish.

In addition to the characteristics mentioned above, the films containing only the babassu mesocarp presented an amber color, which can be related to the presence of tannins [22, 23]. On the other hand, the BM/SA/Gl/Pal films presented a more intense amber color than the BM and BM/SA/Gl films, which can be attributed to the presence of the clay mineral palygorskite in their composition, resulting in a color darker than the others.

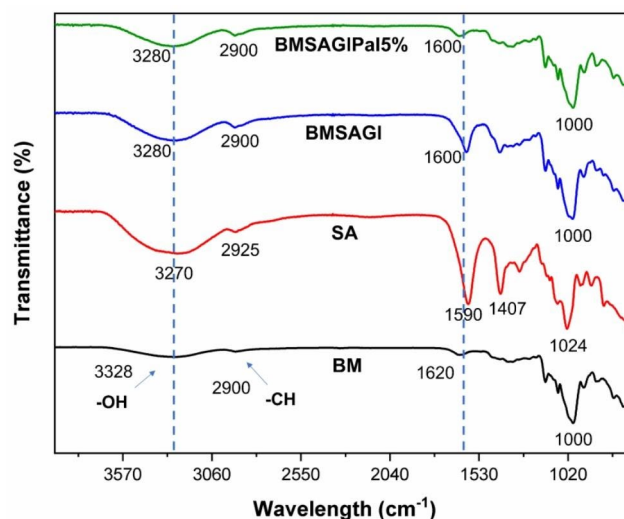


Fig. 3 FTIR spectra of BM, SA, BM/SA/Gl, and BM/SA/Gl/Pal films

Infrared Spectroscopy

The FTIR technique was used to investigate the main groups in the films of BM, SA, BM/SA/Gl, and the BM/SA/Gl/Pal composite.

In the babassu mesocarp spectrum (Fig. 3, black curve), the band observed between 3640 cm^{-1} and 3050 cm^{-1} (maximum at 3328 cm^{-1}) can be attributed to the -OH stretching in alcohol and on the hydroxyl groups of acids. The 2900 cm^{-1} band is attributed to the vibration of the -C-H group. The band at 1620 cm^{-1} is attributed to the stretching in the -C=O (amide I) in proteins present in BM, and this region may indicate the presence of adsorbed water or water groups attached to BM compounds [24]. The 1000 cm^{-1} band corresponds to the vibration of glucose at -C-O-C-. The bands below 1000 cm^{-1} are associated with the absorption of hydroxyl groups in the cellulose monomer [25].

The sodium alginate (SA) film spectrum, in Fig. 3, showed a band at 3270 cm^{-1} that is attributed to the -OH stretch formed by the hydrogen bonds present in SA, while the band around 2925 cm^{-1} is associated with the -CH stretch. The band at 1024 cm^{-1} is related to the -C-O stretch [26]. The bands at 1590 cm^{-1} and 1407 cm^{-1} are characteristic of carboxylate ions in the SA structure.

Figure 3 also shows the spectra of the BM/SA/Gl films and the BM/SA/Gl/Pal composite. In both films, bands like those in the films containing SA and BM appear. Still, the band observed between 3640 cm^{-1} and 3050 cm^{-1} can be attributed to the -OH stretching present in the clay structure, and the band at 3430 cm^{-1} can be attributed to water groups adsorbed on the clay surface. In addition, the presence of Pal in the BM/SA/Gl/Pal composite did not cause significant changes in the film spectrum.

Morphological Study

Figure 4 presents the images of the BM films with a magnification of 500x, 1000x, and 2000x film (Fig. 4A and B, and 4 C). The surface of the BM film can be characterized as an irregular topography, with small white dots that may be related to the presence of non-solubilized starch granules, which may cause structural non-compliance due to their non-gelatinization [27, 28]. In addition, some intact starch granules, which did not break with the formation of the films, are observed; these imperfections can lead to a lower mechanical strength in the films [29].

Images of Babassu Mesocarp films associated with Sodium Alginate (BM/SA/GI) can be seen in Fig. 4 (Fig. 4D F). The surface morphology of BM/SA/GI films presented a more regular topography when compared to BM films. In the images, a coalescence was observed between the materials related to the formation process caused by filmogenic solution viscosity. This behavior corroborates with the results of the analysis of the visual aspect of the films. It is noticed that there is no presence of fissures or cracks in the film, indicating the action of sodium alginate as a plasticizer in BM films. Besides, the surface characteristics in the films can provide more excellent mechanical resistance, as already reported in research in the literature [30].

Figure 4G H present the SEM images of Babassu Mesocarp films associated with sodium alginate with 5% Palygorskite. A smoother surface was observed besides the small granules adhering to the material.

Still, in Fig. 4 (G to I), agglomerates of Pal distributed throughout the polymeric matrix of the film were observed. These aggregates have varied shapes and sizes and are

well-adhered and integrated into the film matrix. The excellent integration between the Pal fibers and the polymeric film can result in interesting mechanical, thermal, and barrier properties [30].

EDS Analysis

Figure 5 shows the BM EDS, in which the main chemical elements constituting the babassu mesocarp, carbon and oxygen, are observed, considering that it is an organic material with about 55% carbon and 44% oxygen. Therefore, these were the elements found in the analysis. And it is possible to observe its uniformity throughout the surface, as shown in Fig. 5.

Figure 5 also shows the EDS of the BM/SA/GI film. The main elements that constitute Sodium Alginate (SA) were observed, which are oxygen (O) and sodium (Na). It can be seen that the SA is well dispersed in the BM matrix, providing a more uniform surface [31], and this uniformity is evidenced by the SEM presented in Fig. 4.

The EDS of the BM/SA/GI/Pal film (Fig. 6) confirmed the presence of a small cluster of Pal. EDS shows the presence of one of the main elements of the palygorskite clay mineral, Silicon (Si). It was observed that the points that evidence the existence of silicon are well distributed in the BM matrix, resulting in a film with better flexibility and visual aspect compared to the BM films.

In the EDS results of the BM/SA/GI/Pal film, Fig. 6, it was also possible to observe the presence of the main elements (O, Na, Si), with the present (Na) coming from SA and the (Si) from clay mineral. In addition, the dispersion and homogeneity of the materials can improve their

Fig. 4 SEM images of BM films with a magnification of 500x (A), 1000x (B), and 2000x (C); BM/SA/GI in 500x (D), 1000x (E), and 2000x (F); and BM/SA/GI/Pal in 500x (G), 1000x (H) and 2000x (I)

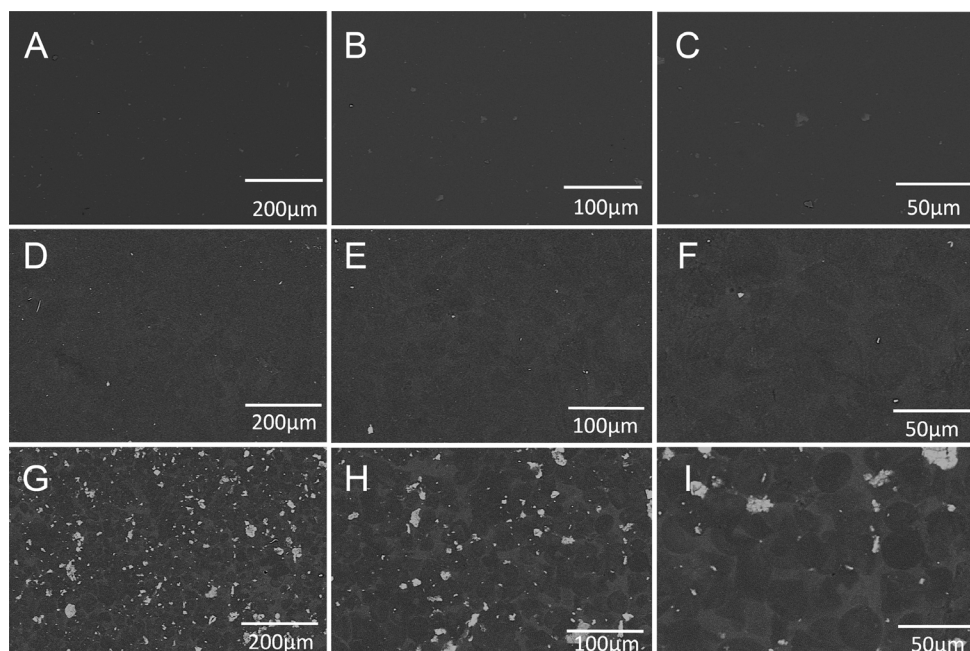
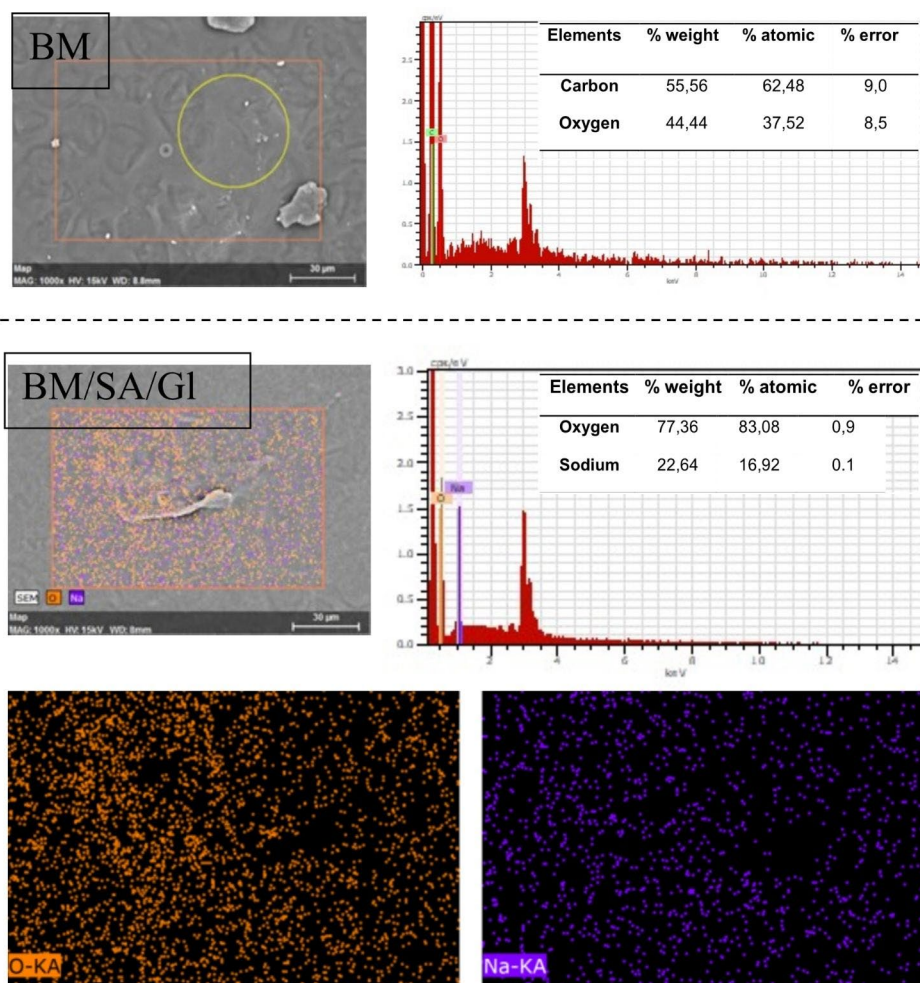


Fig. 5 EDS analysis of BM and BM/SA/GI film



resistance to oxygen and water permeability, which makes the application of the composite in packaging.

Thermal Properties

Figure 7 shows the TGA/DTGA curves of Pal, BM, BM/SA/GI, and BM/SA/GI/Pal.

In Pal's TGA/DTGA curves, Fig. 7, four main mass loss events are observed. The first mass loss occurs with the initial temperature (T_i) of 25.86 °C, final temperature (T_f) of 107.37 °C, and maximum temperature (T_m) of 85 °C, which refers to the loss of physisorbed water and part of the zeolitic waters, this mass loss corresponding to 2.5% [32].

The second mass loss of 1.8% occurs at the initial temperature (T_i) of 107.37 °C, final temperature (T_f) of 204.2 °C, and maximum temperature of 196 °C, which corresponds to thermal dehydration of the rest of the zeolitic water from the Pal structure [33]. The third mass loss of 7% occurs with an initial temperature (T_i) of 204.2 °C, a final temperature (T_f) of 519.2 °C, and a maximum temperature (T_m) of 484 °C,

which is attributed to the loss of coordination water, structural hydroxyls, as well as silanol and luminol groups [34].

The fourth mass loss of 7.3% with initial temperature (T_i) of 519.2 °C, final temperature (T_f) of 797.4 °C, and maximum temperature (T_m) of 708 °C is attributed to dihydroxylation processes of Mg-OH groups from Pal [35]. In this temperature range, the elimination of water molecules also occurs, accompanied by partially destroying the Pal structure. In this temperature range, carbon hydroxide is also released, since above 500 °C, the carbonates present in Pal are thermally unstable, and their decomposition releases CO₂ [36].

The BM TGA/DTGA curves, Fig. 7, have similar profiles to the starch and cellulose curves, confirming the high content of starch, cellulose, lignin, and hemicellulose present in BM [37]. The first stage of mass loss refers to the liberation of water molecules and small masses abundant in carbon or simply the loss of moisture physically absorbed by the sample's surface [38]. This stage corresponds to a mass loss of 13.3% for BM from 25 to 129.5 °C. The second and third

Fig. 6 BM/SA/GI/Pal EDS

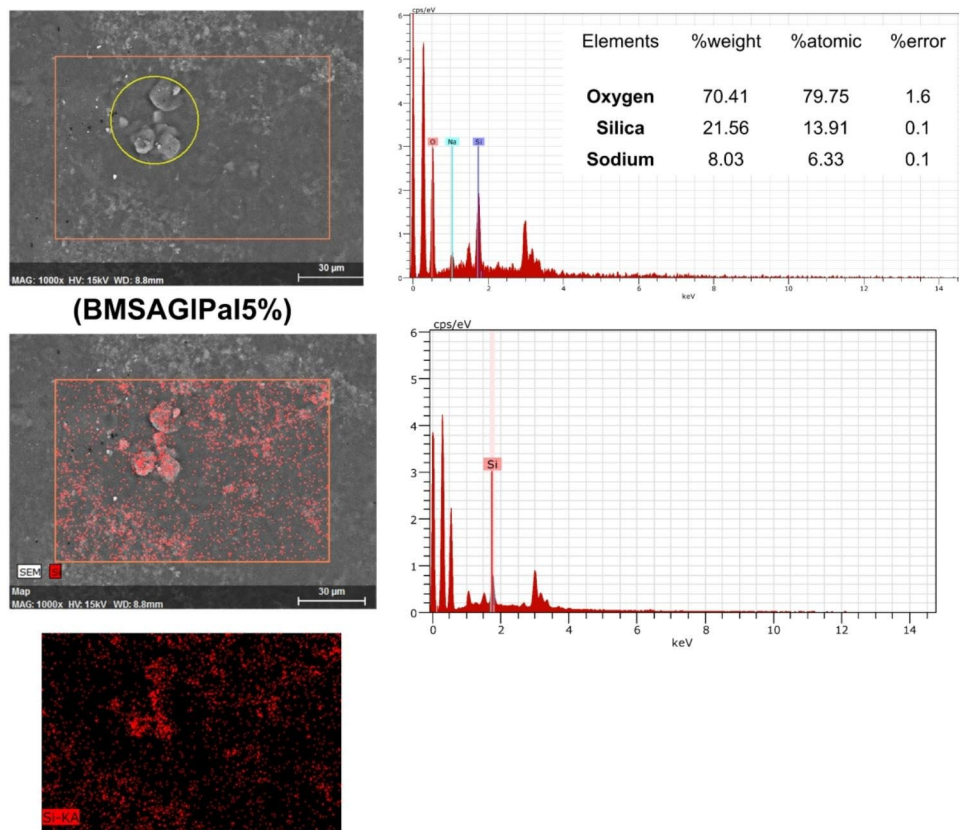
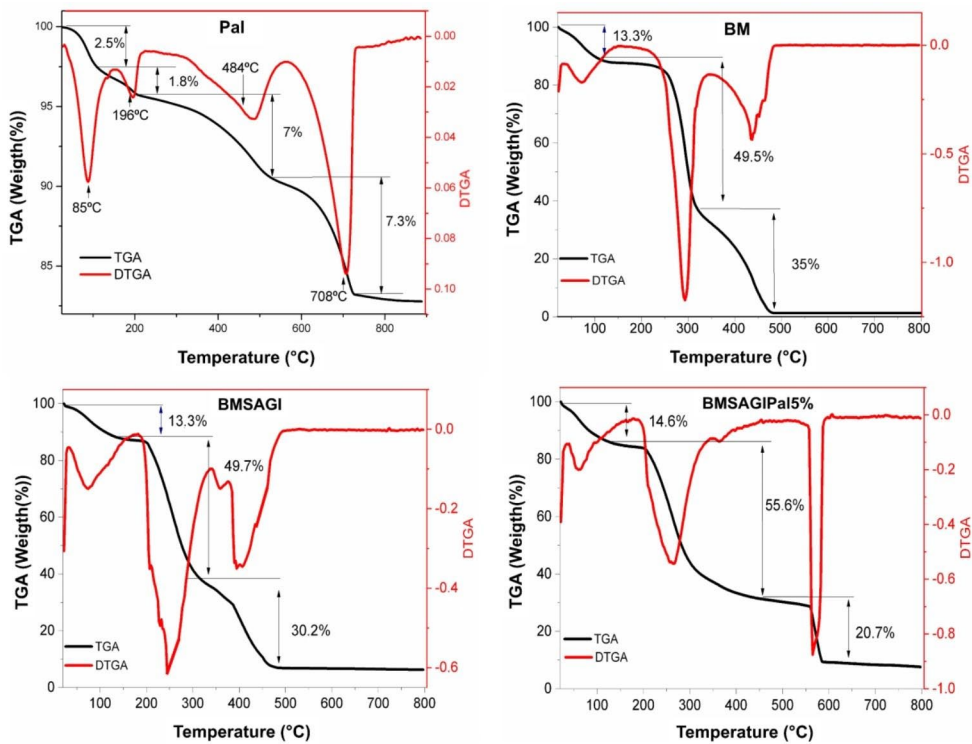


Fig. 7 TGA/DTGA curves of Pal, BM, BM/SA/GI e BM/SA/GI/Pal



stages of mass loss correspond to thermal degradation of hemicellulose and structure BM, which is 49.5% and 35% at BM in the intervals between 129.5 and 316 °C and 316 and 480 °C, respectively [39]. Finally, the BM film showed about 2% of residual ash.

SA and BM degradation events show similarities, with three stages of mass loss at the same temperatures. For the BM/SA/GI film, the first mass loss (13.3%) occurs between 25 and 184.6 °C due to film dehydration. The peak of the DTGA curve confirms this event with a maximum temperature of 77 °C due to the release of water adsorbed on the material [40]. A second significant mass loss (49.7%) is observed in the range from 184.6 to 338.5 °C, which is attributed to the chemisorption of water in the sodium alginate structure and the initial degradation of BM. In the third event, a loss of mass (30.2%) corresponds to the degradation of BM and SA. However, there is no third degradation process of SA.

The BM/SA/GI film residue was 6.8% concerning the initial mass and was obtained after 513 °C; this increase in the residue is due to sodium oxide (NaO₂) from the degradation of SA [41, 42].

The TGA/DTGA curve for the BM/SA/GI/Pal film, Fig. 7, presents three mass loss processes, the first step corresponding to the temperature range from 25 °C to 182.9 °C with a loss of 14.6%, which corresponds to the surface water loss of the film. The second stage of mass loss corresponds to the temperature range from 182.9 to 523 °C, with a loss of 55.6%, which can be attributed to the decomposition of part of the SA and BM. In this stage, too, there is a loss of zeolitic water from Pal, in addition to coordination water from Pal and structural hydroxyls [43].

From the second and third stages, the mass losses of the film BM/SA/GI/Pal in temperature intervals were higher than those of the other two films studied, confirming once again that the composite of BM/SA/GI/Pal has higher thermal stability. The third stage of mass loss included the temperature range between 523 and 660 °C with a loss of 20.7%, corresponding to the degradation of SA and the dihydroxylation of Pal's Mg-OH groups. The residue obtained after 660 °C, where no mass change occurred, was 9.1%, i.e., the film BM/SA/GI/Pal exhibited more excellent

thermal stability than BM and BM/SA/GI, which can be attributed to the presence of the clay mineral palygorskite in the composition of the film. A table describing all events can be found in the supplementary material.

Mechanical Properties

The mechanical properties of the BM, BM/SA/GI films, and the BM/SA/GI/Pal composite are shown in Table 2. In the mechanical properties of tensile strength and elongation to break, a gradual increase in these properties was observed in the films produced. All babassu starch films generally have a low elongation at break and high tensile strength due to amylopectin molecules hindering chain mobility [15].

For the BM film, in Table 2, a lower tensile strength (19.72 MPa) was observed. This behavior is due to the low molecular mobility that makes sliding between the polymer chains difficult. In addition, the low tensile strength is related to fissures and starch agglomerates, identified by SEM images, which are stress concentrators and make the films more fragile.

For the BM/SA/GI film, there was an increase in the values for maximum force, maximum stress, and elongation at break increased compared to the BM film. The increase in these properties can be attributed to the chemical similarity of the materials and the interaction of the hydroxyl groups of BM with the carboxyl groups of SA [44, 45]. Based on the images of SEM, a less rough topography of the BM/SA/GI films was observed compared to the BM film, indicating a more compact material. In the absence of pores, these factors contributed to the increase in tensile strength of this film.

For BM/SA/GI/Pal films, there was an increase of 48%, 46%, and 157% in maximum force, maximum strain, and elongation to rupture, respectively, compared to BM films. This increase can be attributed to the presence of SA and Pal. The increase in these values and, consequently, better mechanical properties of the composite can be attributed to the chemical similarity of the materials and the interaction of the hydroxyl groups of BM with the carboxyl groups of SA and with the silica groups of Pal [46], evidenced in the EDS of the films. In the SEM images, it was possible to identify a surface with irregular topography and good adhesion between the Pal and the matrix. Combined, these factors led to a more excellent mechanical resistance of the BM/SA/GI/Pal film, which is interesting for packaging applications.

The maximum tensile strength for BM/SA/GI/Pal film was 28.8 MPa, a value higher than that observed for some commercial polymers, such as Polyvinyl Acetate (\cong 1.5 to 4.0 MPa) [47, 48], Poly(glycolic acid) (\cong 13.0 MPa) [49], Polycaprolactone (\cong 16.0 MPa) [50, 51], and Poly(hydroxybutyrate) (\cong 25.0 MPa) [52]. In supplementary

Table 2 Mechanical properties of BM, BM/SA/GI, and BM/SA/GI/Pal films

Samples	Force Maximum (N)	Strain Maximum (MPa)	Elongation to rupture (%)	Young's Modulus (MPa)
BM	11.52 ± 1.6	19.72 ± 2.99	1.89 ± 0.33	2024.53 ± 194.46
BM/SA/GI	14.09 ± 1.8	25.56 ± 2.77	3.85 ± 0.70	1756.02 ± 295.26
BM/SA/GI/Pal	16.91 ± 1.5	28.80 ± 2.02	4.85 ± 0.34	2152.08 ± 110.39

Table 3 Moisture content of BM, BM/SA/GI, and BM/SA/GI/Pal films

Films	M_i (g)	M_f (g)	M_c (%)	Standard deviation
BM	0.0315	0.0285	9.5	0.0002
BM/SA/GI	0.0254	0.0233	8.3	0.0007
BM/SA/GI/Pal	0.0347	0.0305	12.1	0.0006

Table 4 Average solubility of BM, BM/SA/GI, and BM/SA/GI/Pal films

Films	M_0 (g)	M_1 (g)	S_w (%)	Standard deviation
BM	0.085	0.025	13.68	0.0012
BM/SA/GI	0.0233	0.017	28.32	0.0005
BM/SA/GI/Pal	0.0300	0.023	24.59	0.0001

material, Table S4 compares the maximum tensile strength between the composite BM/SA/GI/Pal and some commercial polymers [53].

The Young's modulus values obtained for these films were similar. However, a slight increase of 6% and 23% of the BM/SA/GI/Pal film concerning the BM and BM/SA/GI films, respectively.

Study of Moisture Content

The amount of water in the films released through the moisture content analysis is presented in Table 3. The BM films have a moisture content of 9.5%. As for the BM/SA/GI film, approximately 8.3% and the BM/SA/GI/Pal film, which contains the clay mineral Pal, increased moisture content to 12.1%.

The results obtained in this study were similar to those described in the literature for BM flour and BM starch [54]. The increase in the moisture content of the BM/SA/GI/Pal film may be related to water absorption with Pal. On the other hand, the BM/SA/GI film allowed for lower water absorption, and this may be due to the reduction of fissures in the BM matrix, as evidenced by the SEM images.

Solubility in Water Test

The films produced in this study showed lower solubility values than studies carried out for films using BM starch. According to the results of solubility in water presented in Table 4, the BM films showed lower solubility about the films containing sodium alginate and Palygorskite; such behavior may be associated with BM due to its hydrophobicity characteristics. The BM/SA/GI films showed higher water solubility, around 28.32%, probably due to the hydrophilic character of SA and GI, which are completely soluble in water.

The BM/SA/GI/Pal films showed a water solubility of 24.59%, a value lower than the BM/SA/GI film. Compared with other studies [55, 56], these values are similar for collagen-based films associated with Laponite, gelatin-based

films, and cassava starch films, both associated with different concentrations of Laponite. This solubility reduction may be associated with the -OH groups of the matrix and Pal's silanol groups, as shown in the FTIR. The formation of chemical bonds between the clay mineral and the matrix suggests a lower solubility in water, making this material promising for producing films intended for food packaging.

Wettability Study

The contact angle values of BM, BM/SA/GI, and BM/SA/GI/Pal films are presented in Table S2, Supplementary Material. The BM film presented a contact angle of $56.68^\circ \pm 0.68$, indicating a hydrophilic character. However, BM's hydrophobic character may have influenced this film's irregularity, as shown in the SEM images.

The BM/SA/GI film had a contact angle of $101.13^\circ \pm 1.02$, indicating a surface with hydrophobic properties, despite the hydrophilic character of AS. The interactions SA-BM may have increased the packing of BM, reducing the matrix's voids and the material's surface area and a more regular surface (as seen in SEM images). Thus, the hydrophobicity of BM prevailed, and AS contributed to reducing surface irregularities and increasing water solubility.

The measured contact angle for the BM/SA/GI/Pal composite film was $103.98^\circ \pm 0.26$, with a slight increase, compared to the value obtained for the BM/SA/GI, which may be due to the presence of Pal. The BM/SA/GI and BM/SA/GI/Pal films are more hydrophobic than the results described in the literature for the BM starch and pinhão starch films [57] hydrophilic.

The contact angle results for the BM/SA/GI/Pal films corroborate the solubility and moisture content results. Thus, such properties confirm that the composite is attractive for producing films intended for packaging.

Conclusions

The properties evaluated in this study showed the feasibility of forming films by casting using Babassu Mesocarp, Sodium Alginate, Glycerol, and Palygorskite. The films generally presented a uniform color, smooth, shiny surface with no fissures. The FTIR analysis for the BM/SA/GI/Pal film suggested the presence of interactions between the clay and the matrix. In addition, the SEM showed a more regular topography than the other films, more excellent thermal stability, possibly due to the incorporation of Palygorskite, and superior mechanical properties of tensile strength for the composite. Finally, the composite BM/SA/GI/Pal showed lower solubility in water and higher hydrophobicity, making

this material promising for producing films intended for food packaging.

Supplementary Information The online version contains supplementary material available at <https://doi.org/10.1007/s10924-023-03074-8>.

Acknowledgements The authors are grateful for the financial support received; the Research Productivity Grant granted (process 313370/2020-6 (CNPq Call N° 09/2020), and the Master's Scholarship granted by CAPES Agreement.

Author Contributions MVS: writing—original draft, visualization, investigation, formal analysis, validation. RMP: investigation, formal analysis, validation. EAOF: writing—original draft, validation, and writing—review and editing. KRA: formal analysis, visualization. CMA: investigation, formal analysis. CJFB: investigation, formal analysis. RB: formal analysis, visualization. TSA: investigation, formal analysis. LCB: investigation, formal analysis. CE: Funding, writing—original draft, conceptualization, methodology, supervision, writing—review and editing.

Declarations

Competing Interests The authors declare no competing interests.

Conflict of Interest The authors declare that there is no conflict of interest.

References

- Amena S (2022) Utilizing solid plastic wastes in subgrade pavement layers to reduce plastic environmental pollution. *Clean Eng Technol* 7:100438. <https://doi.org/10.1016/j.clet.2022.100438>
- Yang W, Qi J, Arif M et al (2021) Impact of information acquisition on farmers' willingness to recycle plastic mulch film residues in China. *J Clean Prod* 297:126656. <https://doi.org/10.1016/j.jclepro.2021.126656>
- Zhao Z-Y, Wang P-Y, Wang Y-B et al (2021) Fate of plastic film residues in agro-ecosystem and its effects on aggregate-associated soil carbon and nitrogen stocks. *J Hazard Mater* 416:125954. <https://doi.org/10.1016/j.jhazmat.2021.125954>
- La Fuente CIA, Tribst AAL, Augusto PED (2022) Knowledge and perception of different plastic bags and packages: a case study in Brazil. *J Environ Manage* 301:113881. <https://doi.org/10.1016/j.jenvman.2021.113881>
- Liu Y, Liu Z, Guo Z et al (2022) Enhancement of the degradation capacity of IsPETase for PET plastic degradation by protein engineering. *Sci Total Environ* 834:154947. <https://doi.org/10.1016/j.scitotenv.2022.154947>
- Aswathi Mohan A, Robert Antony A, Greeshma K et al (2022) Algal biopolymers as sustainable resources for a net-zero carbon bioeconomy. *Bioresour Technol* 344:126397. <https://doi.org/10.1016/j.biortech.2021.126397>
- Landim APM, Bernardo CO, Martins IBA et al (2016) Sustentabilidade quanto às embalagens de alimentos no Brasil. *Polimeros*. <https://doi.org/10.1590/0104-1428.1897>
- Stloukal P, Kalendova A, Mattausch H et al (2015) The influence of a hydrolysis-inhibiting additive on the degradation and biodegradation of PLA and its nanocomposites. *Polym Test* 41:124–132. <https://doi.org/10.1016/J.POLYMERTESTING.2014.10.015>
- Di Donato P, Taurisano V, Poli A et al (2020) Vegetable wastes derived polysaccharides as natural eco-friendly plasticizers of sodium alginate. *Carbohydr Polym* 229:115427. <https://doi.org/10.1016/J.CARBPOL.2019.115427>
- Chen L, Huang G (2018) The antiviral activity of polysaccharides and their derivatives. *Int J Biol Macromol* 115:77–82. <https://doi.org/10.1016/J.IJBIOMAC.2018.04.056>
- Jiménez-Rosado M, Zarate-Ramírez LS, Romero A et al (2019) Bioplastics based on wheat gluten processed by extrusion. *J Clean Prod* 239:117994. <https://doi.org/10.1016/J.JCLEPRO.2019.117994>
- Baruque Filho EA, Baruque M, da GA, Sant'Anna GL (2000) Babassu coconut starch liquefaction: an industrial scale approach to improve conversion yield. *Bioresour Technol* 75:49–55. [https://doi.org/10.1016/S0960-8524\(00\)00026-2](https://doi.org/10.1016/S0960-8524(00)00026-2)
- Ferrari RA, Soler MP (2015) Obtention and characterization of coconut babassu derivatives. *Sci Agric* 72:291–296. <https://doi.org/10.1590/0103-9016-2014-0278>
- Saraiva Rodrigues SC, da Silva AS, de Carvalho LH et al (2020) Morphological, structural, thermal properties of a native starch obtained from babassu mesocarp for food packaging application. *J Mater Res Technol* 9:15670–15678. <https://doi.org/10.1016/j.jmrt.2020.11.030>
- Maniglia BC, Tessaro L, Ramos AP, Tapia-Blácido DR (2019) Which plasticizer is suitable for films based on babassu starch isolated by different methods? *Food Hydrocoll* 89:143–152. <https://doi.org/10.1016/j.foodhyd.2018.10.038>
- Teepakakorn A, Hayakawa T, Ogawa M (2022) Remarkable stability of dye in polymer-clay nanocomposite film. *Appl Clay Sci* 218:106405. <https://doi.org/10.1016/j.clay.2021.106405>
- Meng Z, Li J, Zou Y et al (2022) Advanced montmorillonite modification by using corrosive microorganisms as an alternative filler to reinforce natural rubber. *Appl Clay Sci* 225:106534. <https://doi.org/10.1016/j.clay.2022.106534>
- Zhang Q, Zhang H, Ding J et al (2022) Preparation, characterization and performance evaluation of chitosan/palygorskite/glycyrrhizic acid nanocomposite films. *Appl Clay Sci* 216:106322. <https://doi.org/10.1016/j.clay.2021.106322>
- Coelho ACV, Santos P, de Santos S (2007) S ARGILAS ESPECIAIS: ARGILAS QUIMICAMENTE MODIFICADAS – UMA REVISÃO Antonio Carlos Vieira Coelho* e Pêrsio de Souza Santos. 30:1282–1294
- de Carvalho Neto AGV, dos Santos DI, Rissato SR et al (2020) Avaliação das propriedades físicas, químicas e mecânicas de Matéria (Rio de Janeiro) 25. <https://doi.org/10.1590/s1517-707620200003.1135>. filmes de amido/PVA/argila bentonita modificados com metacrilato de glicidila
- Alboofetileh M, Rezaei M, Hosseini H, Abdollahi M (2013) Effect of montmorillonite clay and biopolymer concentration on the physical and mechanical properties of alginate nanocomposite films. *J Food Eng* 117:26–33. <https://doi.org/10.1016/j.jfoodeng.2013.01.042>
- Nascimento FRF, Barroqueiro ESB, Azevedo APS et al (2006) Macrophage activation induced by *Orbignya phalerata* Mart. *J Ethnopharmacol* 103:53–58. <https://doi.org/10.1016/j.jep.2005.06.045>
- Alves Lopes I, Coelho Paixão L, Souza da Silva LJ et al (2020) Elaboration and characterization of biopolymer films with alginate and babassu coconut mesocarp. *Carbohydr Polym* 234:115747. <https://doi.org/10.1016/j.carbpol.2019.115747>
- Fabian H, Schultz CP (2000) Fourier transform infrared spectroscopy in peptide and protein analysis. *Encyclopedia of Analytical Chemistry*. John Wiley & Sons, Ltd, Chichester, UK, pp 1–25
- Da Silva DC, Lopes IA, Da Silva LJS et al (2019) Physical properties of films based on pectin and babassu coconut mesocarp.

- Int J Biol Macromol 130:419–428. <https://doi.org/10.1016/j.ijbiomac.2019.02.151>
26. Xiao Q, Gu X, Tan S (2014) Drying process of sodium alginate films studied by two-dimensional correlation ATR-FTIR spectroscopy. *Food Chem* 164:179–184. <https://doi.org/10.1016/j.foodchem.2014.05.044>
 27. Alanís-López P, Pérez-González J, Rendón-Villalobos R et al (2011) Extrusion and characterization of thermoplastic starch sheets from macho Banana. *J Food Sci* 76:E465–E471. <https://doi.org/10.1111/j.1750-3841.2011.02254.x>
 28. Thompson RC, Moore CJ, vom Saal FS, Swan SH (2009) Plastics, the environment and human health: current consensus and future trends. *Philosophical Trans Royal Soc B: Biol Sci* 364:2153–2166. <https://doi.org/10.1098/rstb.2009.0053>
 29. Xie Q, Li F, Li J et al (2018) A new biodegradable sisal fiber–starch packing composite with nest structure. *Carbohydr Polym* 189:56–64. <https://doi.org/10.1016/J.CARBPOL.2018.01.063>
 30. Alcântara ACS, Darder M, Aranda P et al (2015) Bionanocomposites based on polysaccharides and fibrous clays for packaging applications. *J Appl Polym Sci* 133. <https://doi.org/10.1002/app.42362>
 31. Fuzlin AF, Saadiah MA, Yao Y et al (2020) Enhancing proton conductivity of sodium alginate doped with glycolic acid in bio-based polymer electrolytes system. *J Polym Res* 27:207. <https://doi.org/10.1007/s10965-020-02142-0>
 32. Vieira AP, Santana SAA, Bezerra CWB et al (2011) Epicarp and mesocarp of babassu (*Orbignya speciosa*): characterization and application in copper phthalocyanine dye removal. *J Braz Chem Soc* 22:21–29. <https://doi.org/10.1590/S0103-50532011000100003>
 33. Cheng H, Yang J, Frost RL (2011) Thermogravimetric analysis–mass spectrometry (TG-MS) of selected chinese palygorskites—implications for structural water. *Thermochim Acta* 512:202–207. <https://doi.org/10.1016/J.TCA.2010.10.008>
 34. Suárez M, García-Romero E (2006) FTIR spectroscopic study of palygorskite: influence of the composition of the octahedral sheet. *Appl Clay Sci* 31:154–163. <https://doi.org/10.1016/j.clay.2005.10.005>
 35. Boudriche L, Calvet R, Hamdi B, Balard H (2011) Effect of acid treatment on surface properties evolution of attapulgite clay: an application of inverse gas chromatography. *Colloids Surf a Physicochem Eng Asp* 392:45–54. <https://doi.org/10.1016/J.COLSURFA.2011.09.031>
 36. Frost RL, Ding Z (2003) Controlled rate thermal analysis and differential scanning calorimetry of sepiolites and palygorskites. *Thermochim Acta* 397:119–128. [https://doi.org/10.1016/S0040-6031\(02\)00228-9](https://doi.org/10.1016/S0040-6031(02)00228-9)
 37. Maniglia BC, Tapia-Blácido DR (2016) Isolation and characterization of starch from babassu mesocarp. *Food Hydrocoll* 55:47–55. <https://doi.org/10.1016/j.foodhyd.2015.11.001>
 38. Teixeira PRS, Teixeira AS do, Farias NM, de O EA et al (2018) Chemically modified babassu coconut (*Orbignya sp.*) biopolymer: characterization and development of a thin film for its application in electrochemical sensors. *Journal of Polymer Research* 25:127. <https://doi.org/10.1007/s10965-018-1520-8>
 39. Vieira AP, Santana SAA, Bezerra CWB et al (2010) Copper sorption from aqueous solutions and sugar cane spirits by chemically modified babassu coconut (*Orbignya speciosa*) mesocarp. *Chem Eng J* 161:99–105. <https://doi.org/10.1016/j.cej.2010.04.036>
 40. Iwata T (2015) Biodegradable and bio-based polymers: future prospects of eco-friendly plastics. *Angewandte Chemie - International Edition* 54:3210–3215. <https://doi.org/10.1002/anie.201410770>
 41. Santana SAA, Vieira AP, da Silva Filho EC et al (2010) Immobilization of ethylenesulfide on babassu coconut epicarp and mesocarp for divalent cation sorption. *J Hazard Mater* 174:714–719. <https://doi.org/10.1016/j.jhazmat.2009.09.109>
 42. Santana ACSGV, Sobrinho JLS, da Silva Filho EC, Nunes LCC (2017) Obtaining the palygorskite:chitosan composite for modified release of 5-aminosalicylic acid. *Mater Sci Engineering: C* 73:245–251. <https://doi.org/10.1016/j.msec.2016.12.068>
 43. Ogorodova L, Vigasina M, Melchakova L et al (2015) Thermochemical study of natural magnesium aluminum phyllosilicate: Palygorskite. *J Chem Thermodyn*. <https://doi.org/10.1016/j.jct.2015.05.023>
 44. Amin MR, Chowdhury MA, Kowser MA (2019) Characterization and performance analysis of composite bioplastics synthesized using titanium dioxide nanoparticles with corn starch. *Heliyon* 5:e02009. <https://doi.org/10.1016/J.HELIYON.2019.E02009>
 45. Li K, Zhu J, Guan G, Wu H (2019) Preparation of chitosan-sodium alginate films through layer-by-layer assembly and ferulic acid crosslinking: Film properties, characterization, and formation mechanism. *Int J Biol Macromol* 122:485–492. <https://doi.org/10.1016/j.ijbiomac.2018.10.188>
 46. Carazo E, Borrego-Sánchez A, García-Villén F et al (2018) Adsorption and characterization of palygorskite-isoniazid nanohybrids. *Appl Clay Sci* 160:180–185. <https://doi.org/10.1016/J.CLAY.2017.12.027>
 47. Kokabi M, Sirousazar M, Hassan ZM (2007) PVA–clay nanocomposite hydrogels for wound dressing. *Eur Polym J* 43:773–781. <https://doi.org/10.1016/j.eurpolymj.2006.11.030>
 48. Youssef HF, El-Naggar ME, Fouda FK, Youssef AM (2019) Antimicrobial packaging film based on biodegradable CMC/PVA-zeolite doped with noble metal cations. *Food Packag Shelf Life* 22:100378. <https://doi.org/10.1016/j.foodpsl.2019.100378>
 49. Samantaray PK, Little A, Haddleton DM et al (2020) Poly(glycolic acid) (PGA): a versatile building block expanding high performance and sustainable bioplastic applications. *Green Chem* 22:4055–4081. <https://doi.org/10.1039/D0GC01394C>
 50. Jost V (2018) Packaging related properties of commercially available biopolymers – an overview of the status quo. *Express Polym Lett* 12:429–435. <https://doi.org/10.3144/expresspolymlett.2018.36>
 51. Shaikh S, Yaqoob M, Aggarwal P (2021) An overview of biodegradable packaging in food industry. *Curr Res Food Sci* 4:503–520. <https://doi.org/10.1016/j.crf.2021.07.005>
 52. Abdelwahab MA, Flynn A, Chiou B-S et al (2012) Thermal, mechanical and morphological characterization of plasticized PLA–PHB blends. *Polym Degrad Stab* 97:1822–1828. <https://doi.org/10.1016/j.polymdegradstab.2012.05.036>
 53. Zhang M, Biesold GM, Choi W et al (2022) Recent advances in polymers and polymer composites for food packaging. *Mater Today* 53:134–161. <https://doi.org/10.1016/j.mattod.2022.01.022>
 54. Maniglia BC, Tessaro L, Lucas AA, Tapia-Blácido DR (2017) Bioactive films based on babassu mesocarp flour and starch. *Food Hydrocoll* 70:383–391. <https://doi.org/10.1016/j.foodhyd.2017.04.022>
 55. Perez V, Felix M, Romero A, Guerrero A (2016) Characterization of pea protein-based bioplastics processed by injection moulding. *Food Bioprod Process* 97:100–108. <https://doi.org/10.1016/J.FBP.2015.12.004>
 56. Valencia GA, Lourenço RV, Bittante AMQB, do Amaral Sobral PJ (2016) Physical and morphological properties of nanocomposite films based on gelatin and laponite. *Appl Clay Sci* 124–125:260–266. <https://doi.org/10.1016/j.clay.2016.02.023>
 57. Dias AB, Müller CMO, Larotonda FDS, Laurindo JB (2010) Biodegradable films based on rice starch and rice flour. *J Cereal Sci* 51:213–219. <https://doi.org/10.1016/j.jcs.2009.11.014>

Springer Nature or its licensor (e.g. a society or other partner) holds exclusive rights to this article under a publishing agreement with the author(s) or other rightsholder(s); author self-archiving of the accepted

manuscript version of this article is solely governed by the terms of such publishing agreement and applicable law.